Title: Multi-Decadal Improvement in U.S. Lake Water Clarity

Authors: Simon N. Topp*[1], Tamlin M. Pavelsky[1], Emily H. Stanley[2], Xiao Yang[1], Claire G. Griffin[3], Matthew R.V. Ross[4]

Affiliations:

[1] Department of Geological Sciences, University of North Carolina at Chapel Hill

[2] Center for Limnology, University of Wisconsin-Madison

[3] Department of Environmental Sciences, University of Virginia

[4] Department of Ecosystem Science and Sustainability, Colorado State University

*Correspondence to: sntopp@live.unc.edu

Twitter: @simonNtopp

Keywords: Lake clarity, remote sensing, macroscale ecology

This manuscript is a non-peer reviewed pre-print submitted to EarthArXiv.

Title: Multi-Decadal Improvement in U.S. Lake Water Clarity

Authors: Simon N. Topp*[1], Tamlin M. Pavelsky[1], Emily H. Stanley[2], Xiao Yang[1], Claire G. Griffin[3], Matthew R.V. Ross[4]

Affiliations:

[1] Department of Geological Sciences, University of North Carolina at Chapel Hill

[2] Center for Limnology, University of Wisconsin-Madison

[3] Department of Environmental Sciences, University of Virginia

[4] Department of Ecosystem Science and Sustainability, Colorado State University

*Correspondence to: sntopp@live.unc.edu

Keywords: Lake clarity, remote sensing, macroscale ecology

Abstract

Across the globe, recent work examining the state of freshwater resources paints an increasingly dire picture of degraded water quality. However, much of this work either focuses on a small subset of large waterbodies or uses *in situ* water quality datasets that contain biases in when and where sampling occurred. Using these unrepresentative samples limits our understanding of landscape level changes in aquatic systems. In lakes, overall water clarity provides a strong proxy for water quality because it responds to surrounding atmospheric and terrestrial processes. Here, we use satellite remote sensing of over 14,000 lakes to show that lake water clarity in the U.S. has increased by an average of 0.52 cm yr^{-1} since 1984. The largest increases occurred prior to 2000 in densely populated catchments and within smaller waterbodies. This is consistent with observed improvements in water quality in U.S. streams and lakes stemming from sweeping environmental reforms in the 1970s and 1980s that prioritized point-source pollution in largely urban areas. The comprehensive, long-term trends presented here emphasize the need for representative sampling of freshwater resources when examining macroscale trends and are consistent with the idea that extensive U.S. freshwater pollution abatement measures have been effective and enduring, at least for point-source pollution controls.

Introduction

Recent large-scale studies of the aquatic ecosystems have been facilitated by a growing number of easy to use to global (1) and sub-continental (2–4) datasets of field water quality measurements. However, research into one of the largest such datasets (2) suggests that historical field samples tend to be biased towards larger, problematic waterbodies and often lack the temporal continuity necessary for detecting long term trends (5). Using this unrepresentative data to understand regional to national scale lake dynamics can lead to significantly different results when compared to statistically-representative samples (6,7). While this problem of representativeness is increasingly acknowledged in sampling efforts (e.g., the U.S. National Lake Assessment; NLA) (8) systematic sampling programs are costly, can have limited temporal resolution and continuity, and require compromise between scientific rigor and logistical practicality (9). No such sampling program is available at continental scales over multiple decades.

One response to the challenges represented by field studies is to use remote sensing to estimate water quality parameters. Over the past decade, inland water quality remote sensing research has increasingly focused on larger spatial and temporal domains in order to address challenging science questions (10–12). Here, we use remote sensing to conduct the first multi-decadal, national-scale assessment of U.S. lake water clarity by developing a carefully validated data-driven model that is generalizable across more than three decades for the entire contiguous U.S. We calculate regional summer lake water clarity trends from 1984-2018 across nine U.S. ecoregions in two different samples of lakes: a statistically stratified sample (n = 1,029 lakes) defined by the 2012 NLA (13) and a large random sample (n = 13,362 lakes) from the National Hydrography Dataset (NHD) (14). We compare the overarching trends from these remotely-sensed estimates to each other and to the entirety of the available *in situ* data from the Water Quality Portal (WQP) (3) and LAGOS-NE (2), which jointly have over 1 million field observations of U.S. lake clarity dating back to 1984. In doing so we observe the impact of different sampling approaches and illustrate the biases that exist when using historical field samples to identify long term trends. To complement the ecoregion analysis and compare our work to existing studies focusing on larger lakes (11), we add all U.S. lakes larger than 10 km^2 to our NLA and random samples and examine trends in lakes with over 25 years of observations (n = 8,897) to identify how lake-specific trends vary with lake size and population density.

Materials and Methods

Data Processing and Acquisition

Data for model training and validation was derived from a variant of the AquaSat database (15) which combines historical water quality measurements from the Water Quality Portal (3) and LAGOS-NE (2) with coincident (+/- 1 day) satellite images from the USGS tier 1 surface reflectance collections for Landsat 5, 7, and 8. While the atmospheric corrections used to generate these surface reflectance products were originally developed for terrestrial applications, a growing body of research shows that they can be used to accurately estimate inland water quality parameters and perform on par with water-specific atmospheric correction algorithms (16–18). Site IDs from AquaSat were spatially joined to lake polygons from NHDPlusV2 (14) (NHD) and then linked to catchment level metrics from the LakeCat database (19). From the initial AquaSat database, observations were removed if:

- they did not coincide with a lake polygon from NHDPlus V2
- over half of the water pixels within 120 meters of the sample site were classified as anything other than high confidence water by the USGS Dynamic Surface Water Extent water mask (20)
- the Landsat scene contained over 50% cloud cover
- one or more Landsat bands was beyond a reasonable reflectance for water (0-0.2)
- the Fmask (21) indicated the presence of clouds, cloud shadows, or ice over the sample site
- the observation was impacted by topographic shadow
- recorded field water clarity (measured as Secchi disk depth) was < 0.1 meters or > 10 meters (the limits used for the NLA field sampling).

- two identical clarity observations occurred on the same day within the same lake as a result of duplication between WQP and LAGOS-NE (WQP observations were kept while LAGOS-NE observations were removed in these circumstances)

Similarly, reflectance values for analyzing national clarity trends were calculated using the same filters and methodology described above using the lake center as the sample point and taking the median value of high confidence water pixels within 120 meters for all study lakes. As an additional test, the predictions using lake center median values were compared with predictions using whole lake median values for the 2012 NLA lake sample. The two sets of predictions showed strong agreement ($R^2 = 0.95$, Figure S1), so lake centers were used for consistency with AquaSat's point based method. All reflectance values were extracted from Google Earth Engine (22) for the three samples of interest within the study: the statistically stratified NLA 2012 sample (n = 1,038), a large random sample of 2,000 lakes per ecoregion (n = 18,000), and all lakes greater than 10 km^2 (n = 1,170).

Each subsample contained a portion of lakes that were ultimately removed through the quality control measures described above. Spot checking of the removed waterbodies revealed that the most common cause for removal was lack of Landsat visible pure water pixels caused by either irregular waterbody shape (long and narrow), surface vegetation on the waterbody, overhanging vegetation along the shoreline, or a misclassification of a lake within NHD. Removal of these waterbodies led to total lake counts of 1,029 for the NLA sample, 13,362 for the random sample, and 1,105 for lakes over 10 km^2 (for a total of 14,971 unique lakes). While conservative, this filtering approach ensured minimal error from mixed pixels, sun glint, and surrounding adjacency effects from nearby land.

Reflectance values from the differing Landsat sensors were normalized following Gardner et al (2020) (23). For each satellite pair (Landsat 5/7 and Landsat 7/8), the reflectance values observed over the entirety of the NLA sample of lakes were first filtered to coincident time periods when both sensors were active (1999-2012 for Landsat 5 and 7 and 2013-2018 for Landsat 7 and 8). We assume that the distribution of collected reflectance values for a given band should be identical given a sufficient number of observations over the same array of targets regardless of sensor. Based on this assumption, we calculated the 1^{st}-99^{th} reflectance percentiles for each sensor/band during periods of coincident satellite activity. Since Landsat 7 spans the time periods of both Landsat 5 and Landsat 8, each band in 5 and 8 was corrected to Landsat 7 values through a 2^{nd} order polynomial regression of the 1^{st}-99^{th} percentiles of reflectance values between the two sensors for the overlapping time period (Figure S2). The resulting regression equations were then applied to all Landsat 5 and 8 values within AquaSat as well as for all the included study lakes. Ultimately, applying these corrections to the reflectance values reduced the final model mean absolute error by 0.2 meters, suggesting that standardizing the reflectance values between sensors successfully reduced errors from sensor differences.

Application of the above quality control measures for AquaSat resulted in a model training and testing database of 250,760 observations of Secchi Disk depth, associated Landsat reflectance, and site specific lake and catchment properties for an optically diverse sample of waterbodies across the United States dating back to 1984 (Figure S3). Reflectance values for specific bands and band ratios within the training dataset were analyzed for correlations with atmospheric optical depth derived from the MERRA2 reanalysis data (24). Correlations were examined both over the entire study period and between 1991 and 1993, when aerosol optical depth values were particularly high due to the eruption of Mt. Pinatubo. Optical parameters that showed the least correlation to atmospheric optical depth ($r < 0.15$ during 1992 and 1993 and $r < 0.1$ for the study period) were then chosen for inclusion in the modelling pipeline. These included Blue/Green and Nir/Red ratios and the dominant wavelength as described by Wang et al. (2015) (25).

Of the non-optical parameters from the LakeCAT database, we included those that could impact water clarity and were mostly static over time (Table S1). Static 2006 values for catchment level percent impervious surfaces, percent urban landcover, percent forested landcover, percent cropland, and percent wetland landcover were included despite potentially being unrepresentative of the entire study period in some catchments. These variables were deemed important based on existing research (26,27), domain expertise, and various preliminary empirical tests of feature importance, and therefore were included in the modelling pipeline. All lake and landscape-level variables were rounded to the nearest tenth or whole number, depending on the variable scale, in order to prevent certain variables from acting as location identifiers and to avoid overfitting during model training. This initial reduction in the feature space of the training dataset resulted in three optical variables and 27 static lake/landscape variables for each AquaSat matchup observation.

Model Development and Validation

Non-parametric, supervised machine learning algorithms are increasingly popular within the remote sensing community due to their robustness, ease of use, and relatively low computational requirements (28). Among these algorithms, extreme gradient boosting (Xgboost) has been shown to outperform similar non-parametric classification and regression schemes for urban land cover classification (29), determining aerosol optical depth (30), and modeling solar radiation (31). Xgboost classifiers are ensemble models that combine a suite of 'weak' classifiers in order to minimize overall error. Within each iteration, estimates with large errors from the previous iteration are weighted in order to force the model to maximize its performance on the most challenging calibration data. The iterations are additive, meaning that the final model is the sum of the previously weighted regressions.

In order to avoid model overfitting and limit the final number of input variables, we incorporated forward feature selection (FFS) (32) with target oriented leave-location-leave-time out cross validation (LLLTO-CV)(33) into our Xgboost model development. FFS and LLLTO-CV effectively reduce overfitting by cross-validating the model on locations and times not used for model training and removing variables with high spatial or temporal correlations with observed clarity. We set aside 20% of the training dataset (n = 50,153) to use for post-development model testing and trained our initial model with the remaining 80% (n=200,607) using FFS and LLLTO-CV. This process reduced the overall number of input variables from 30 to 11 (3 optical properties and 8 static lake/landscape variables) (Table S1). Finally, the hyperparameters of the model were tuned using a grid search approach with conservative hyperparameter values. To better understand how each input feature contributed to the final model predictions, we calculated the feature importance and accumulated local effects (ALE) (34) for all model inputs (Figure S4). ALE values represent the average marginal impact of a feature on final predictions as the feature value increases or decreases.

Annual Lake Water Clarity Predictions

Lake observations downloaded from Google Earth Engine were limited to those between May and September in order to remove the influence of snow and ice while maximizing the number of cloud free images captured. For any given lake and year, the median of all cloud free predictions was taken as representative of summer lake clarity. These summer clarity predictions were then averaged across the nine ecoregions defined within the NLA to generate estimates of annual regional water clarity. For the NLA sample of lakes, this process led to an average of 883 observations spread across 103 lakes being averaged for each regional estimate of summer water clarity.

Model error was propagated into the mean regional estimates through 1000 iterations of bootstrap sampling. Within each iteration, annual lake median values within each region were sampled with replacement, and the new subsample was used to calculate the annual mean for the region. This bootstrapping procedure effectively propagates a different amount of model noise into each estimate of mean summer clarity by incorporating a different sample of lakes into each iteration of the regional estimate. This resampling results in a distribution of 1000 estimates of clarity for each year/region. Confidence bounds depicted in Figure 2 represent the mean and 90% confidence interval of the bootstrapping procedure.

In order to analyze overarching regional trends, we calculated Thiel-Sen Slopes for each of the generated time series based on the mean of the bootstrap sampling procedure. Thiel-Sen Slope is a nonparametric measure of the magnitude of monotonic trends that is insensitive to outliers within the dataset (35). It determines overall trends by calculating slopes between each pair of points in a time series and then taking the median of all slopes. It is often used in conjunction with Mann-Kendall trend analysis to quantify the more binary Mann-Kendall tau statistic (36). The trends presented here are based on the full remote sensing time series; however, we also calculated trends excluding the years in which atmospheric optical depth was potentially impacted by the Mt. Pinatubo eruption (1991-1993). Overall trends using the filtered timeseries showed only minor differences from the full-time series (Figure S5) indicating that the reported patterns observed here are not artefacts of the abnormal atmospheric conditions in the early 1990s. Trends for the field data were analyzed using the same method as the remote sensing predictions by first taking the summer median of each sampling point, averaging the median values by year/region, and calculating Thiel-Sen slopes from the resulting regional estimates.

Finally, we identified lakes with more than 25 years of observations to conduct lake-scale analysis ($n = 8,897$). We calculated Thiel-Sen Slopes for each individual time series of median summer clarity to examine the distribution of trends at the lake scale. Individual lake trends were binned by lake size and catchment population density to analyze the impact of these lake characteristics on overall clarity trends. The resulting distributions across size classes and catchment population density showed longer tails towards positive trends and were therefore analyzed using non-parametric Mann-Whitney tests rather than the more common parametric t-test. While we did not explicitly propagate model error into these individual lake time series, we attempt to reduce the impact of model noise by examining distributions rather than individual lakes and calculating the median trend for each binned distribution.

Results:

Model Validation:

Validation of our data-driven remote sensing model (Figures 1, S6) indicates that it performs on par with existing regional remote sensing models developed using either traditional regression methods or semi-analytical modelling (12,37,38). However, unlike previous regional

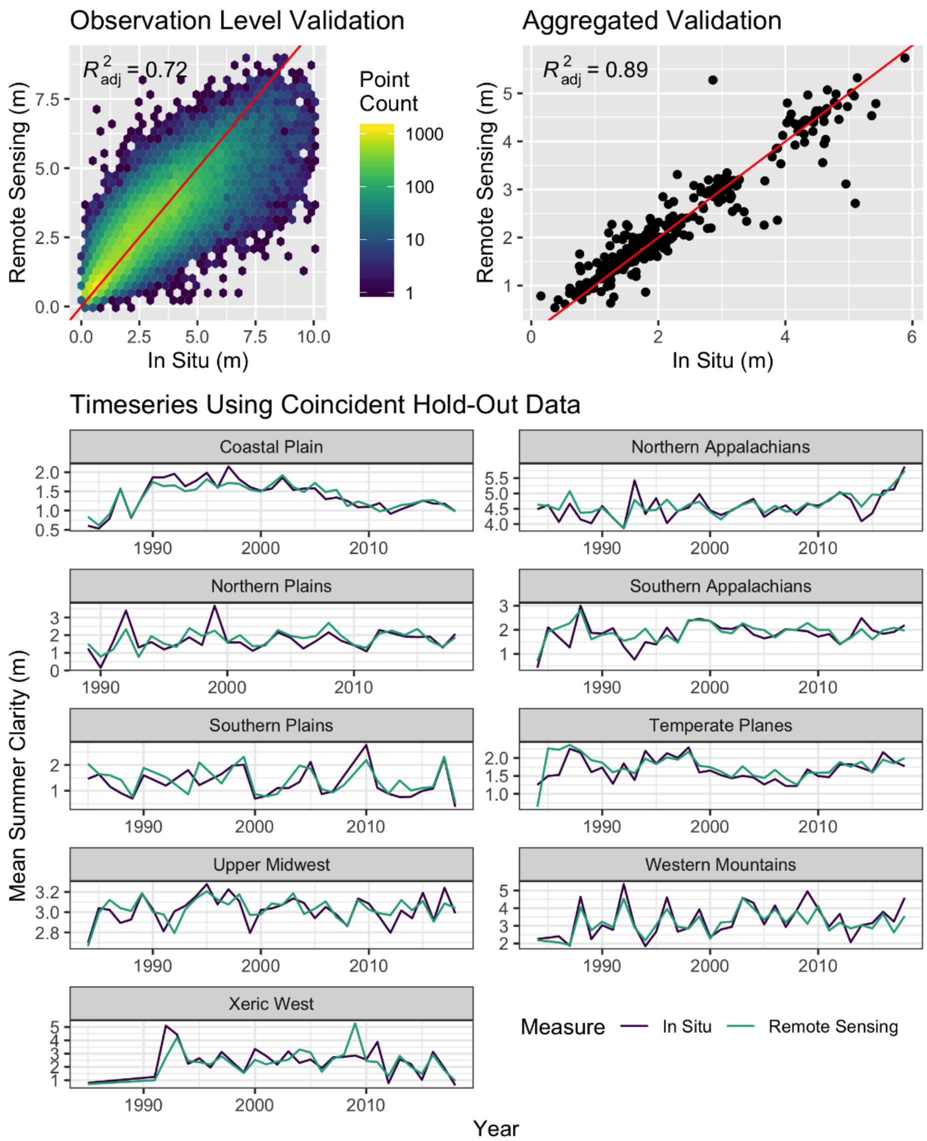

Figure 1. Model validation based on hold-out data not used in model development. Clockwise from the upper left: Point based model performance, model performance aggregated by year and region, and regional timeseries of aggregated validation. Note that the time series shown only include hold-out estimates coincident with field measurements used for validation and do not represent the final time series of the study. They are provided to illustrate that the validation captures regional temporal patterns seen in the field data.

models that are only applicable to a specific scene, sensor, or area, the model presented here is generalizable for over three decades for the entire contiguous United States. Model error was calculated using the hold-out data (n=50,153) not used in model training. Error metrics were calculated at the observation level as well as at the aggregated ecoregion level used in the final analysis. Examination of the model residuals shows a consistent normal distribution over time. This is important both because it reaffirms the sensor correction procedure described above and because it leads to more accurate regional estimates, as over and underpredictions cancel each other out. Observation level error metrics for the final model include a mean absolute error of

0.71 meters (mape = 38%) and bias of 0.004 meters. Regional/annually aggregated error metrics include a mean absolute error of 0.25 meters (mape = 14%) and a bias of -0.02 meters. Feature importance, measured as gain (i.e. the improvement in accuracy when a given feature is included), shows that optical variables, especially the dominant wavelength, contribute the most predictive capability to the model (Figure S4). To further validate the contribution of optical variables to the model, we validated a second, purely optical model on the same training and testing data which resulted in an RMSE of 1.3 m and R^2 of 0.5, indicating that the optical parameters contributed to nearly 70% of the explained variance within the final combined landscape model (with the remaining 30% explained by static lake and landscape characteristics).

Model performance was also broken down by lake size, satellite, data source, and time to ensure that predicted trends were not artefacts of lake or sensor characteristics (Figure S6). While variations in model fit across lake sizes, sensors, and data sources are nominal, the validation did show a slight increase in bias over time, with clarity in earlier years being slightly overpredicted on average and clarity in later years being slightly underpredicted. However, if anything, this small change in bias over time makes our trend predictions conservative as later years are generally underpredicted. We included a breakdown by data source because LAGOS-NE field measurements are all geolocated to lake center points while WQP uses explicit sampling site coordinates (15). For observations recorded in both, we deferred to WQP because of the spatial specificity. However, validation results from both datasets show strong agreement, likely because the vast majority of lakes are small enough that there is minimal variation between lake center points and nearby sampling locations. This similarity also supports the above stated decision to predict clarity based on median center point reflectance values rather than median whole lake reflectance values.

As an additional check, we conducted two comparisons of model performance against known benchmarks in the field. First, we compared our regional estimates of lake water clarity to those of the 2007 and 2012 National Lake Assessments and found strong agreement between the reported field values and our model predictions (mape = 17.7%) (Figure S7). Second, we generated mean summer predictions for the individual lakes included in LakeBrowser (12), a well-validated water clarity remote sensing project focused on over 10,000 lakes in Minnesota (https://lakes.rs.umn.edu/). Comparison of the predictions from the two modelling approaches show agreement when comparing annual estimates at the ecoregion level used by LakeBrowser (R^2 = 0.82) and when compared to field data from the WQP and LAGOS-NE (Figure S8).

Trends in U.S. Lake Water Clarity

Time series generated for the NLA sample of lakes show that, on average, water clarity in U.S. lakes increased at a rate of 0.52 cm yr^{-1} from 1984-2018 (Figure 2). Seven of the nine NLA ecoregions show significant positive trends ($p < 0.05$) that varied from 0.23 cm yr^{-1} ($p = 0.040$) in the Coastal Plains to 1.00 cm yr^{-1} ($p < 1e^{-5}$) in the Northern Appalachians. Significant trends were absent in the Southern Appalachian and Southern Plains regions, but no region had a significant decline in clarity.

Interannual variations in percent clarity change between ecoregions are significantly correlated ($p < 0.05$) in 24 of the 36 (67%) possible region pair combinations (Figure S9). Additionally, during 29% (n=10) of the observed years, at least eight of the nine ecoregions showed synchronous increases or decreases in clarity compared to the previous year. While some

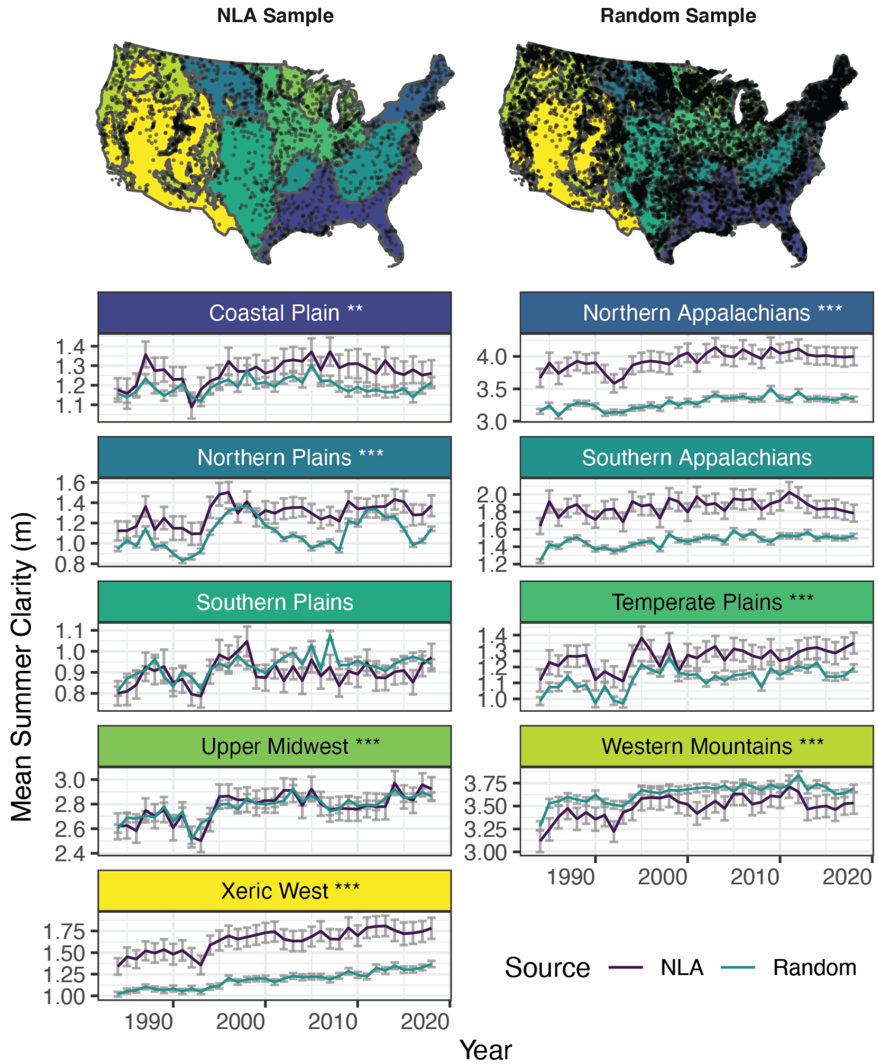

Figure 2. Regional modelled trends in water clarity for the statistically stratified sample of NLA lakes that are Landsat visible and a large random sample of Landsat visible lakes. Trends and their associated confidence intervals represent the mean and standard deviation of values calculated through 1000 iterations of bootstrap sampling of the NLA and random sample lakes respectively. Points on maps represent individual lakes included in the sample. Asterisks indicate significance levels of trends determined by Thiel-Sen slopes at 90% (*), 95% (**), and 99% (***) confidence levels for the NLA sample of lakes.

of these years line up with discrete events (e.g., 1987 was heavily impacted by the Pacific Decadal Oscillation), ascribing this synchrony to specific climatological or anthropogenic drivers is difficult due to the multiscale controls on lake water clarity (26,39). However, the scale of the changes suggests that drivers of water clarity function at national scales for at least some parts of the study period.

Impacts of lake size and population

Recent studies of large-scale drivers of inland water quality suggest both that 1) a variety of anthropogenic and climate forcings are leading to an increase in algal blooms and concomitant decreases in water clarity in many lakes (11,40), and that 2) nutrient loading of U.S. rivers, particularly near urban areas, is decreasing (41,42), a trend that should translate to decreased algal growth in downstream waters, particularly if these receiving systems have relatively short mean water residence times or are isolated from non-point sources of nutrient inputs (43,44). These contradictory narratives may reflect limited use of representative samples at large spatial scales, with most studies systematically under-sampling smaller waterbodies despite their numerical dominance and ecological significance (45).

To better compare our analysis to previous work focusing on larger lakes and river systems, we generated annual water clarity time series for all U.S. lakes larger than 10 km^2 (n = 1,105) in addition to our NLA and random samples to create a full dataset of 14,971 unique lakes. From this sample, we selected only those lakes with at least 25 years of cloud-free remote sensing observations (n_{lakes} = 8,897 lakes, $n_{observations}$ = 2,727,021) and binned them by size class (<1, 1-10, 10-100, and >100 km^2) and catchment population density (20% quantiles) to compare how trends differed by lake size and examine potential links to improving stream water quality in urban areas. The resulting distributions of trends show that the most significant clarity improvements are occurring in smaller waterbodies and in densely populated areas (Figure 3). Lake size and population density are not significantly correlated, nor are these results related to differences between natural lakes and reservoirs, which show no significant difference in their distribution of trends (p = 0.69). For lake size, median trends for lakes in the smallest to largest

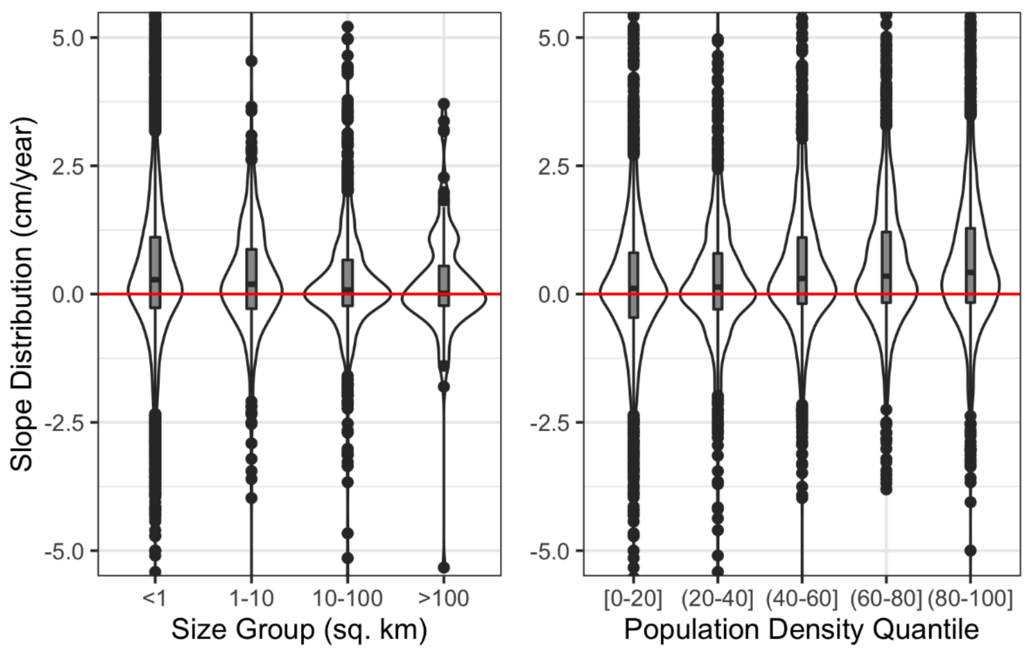

Figure 3. Distribution of modelled trends in lakes with greater than 25 years of observations by (left) lake size class (<1 km^2, n= 7,339; 1-10 km^2, n=509; 10-100 km^2, n= 925; >100 km^2, n=124) and (right) 2010 catchment population density quantiles. Actual values for quintiles in terms of people per km^2: [0-1], (1-3], (3-11], (11-43], (43, 3,970]. Y-axis limits set to -5 to 5 for visualization.

size classes are 0.28, 0.19, 0.08, and 0.02 cm yr^{-1}, respectively, with all but the last class significant at a 99% confidence level. Trends for lakes in catchments within the lowest population density quintile (20%) were approximately four times smaller than for lakes in the most urban upper quintile ($p = 2.2e^{-16}$). Given these trends and the important controls of population density and lake size, research focusing primarily on large lakes may accurately find that water clarity is not increasing. However, the more systematic analysis presented here provides a more complex story in which clarity dynamics are dependent on lake-specific limnological and geographic attributes.

Sampling impact on patterns of water clarity

To examine the effect of lake sampling on observed patterns in water clarity, we replicated our NLA analysis using: 1) remote sensing estimates for a large random sample of lakes (n = 13,362, Figure 2), and 2) the entirety of field data from both LAGOS-NE and WQP, two of the largest national field databases of water quality in the U.S (n = 1,296,659 observations between 1984 and 2018). Results of this comparison show that the NLA sample of lakes accurately reflects temporal patterns of lake clarity across ecoregions compared to a random sample, with some minor geographical exceptions (Figure 2). Regardless of these differences, regional temporal patterns in water clarity are highly correlated between the NLA and random samples, with Pearson's Correlation Coefficients ranging from 0.55 ($p = 5.4e^{-4}$) in the Southern Plains to 0.91 in the Upper Midwest ($p = 1.0e^{-5}$). These high correlations between samples suggest that the NLA sample is representative of a larger random sample of lakes and that observed trends are insensitive to lake sampling given a large enough sample size and regular sampling intervals.

Conversely, comparison of the remotely sensed NLA and large random samples to historical field observations from LAGOS-NE and WQP reveals substantial discrepancies in overall trends (Figure 4). Time series of historical regional clarity calculated with the full set of field data lack significant correlations ($p < 0.01$) with the time series from the NLA sample in seven of the nine study regions. Slopes differ by orders of magnitude from the closely-matched random and NLA samples, in some cases with significant trends in the opposite direction. These results emphasize that conducting an identical analysis with spatiotemporally inconsistent and potentially *ad hoc* field sampling leads to substantially different trends in water clarity compared to the same analysis using representatively sampled remote sensing estimates.

Discussion

Our analysis of long-term trends in lake water clarity across the United States highlights that:

1. Overall clarity in U.S. lakes increased between 1984 and 2018. This increase was concentrated largely in lakes smaller than 10 km^2 and in more urban areas.
2. A systematic understanding of national patterns in lake water clarity requires a representative sample of lakes. These macrosystem-level patterns are not reflected in aggregated historical field data.

By applying our model across both the NLA sample of lakes and a larger random sample, we successfully capture long-term patterns in U.S. lake water clarity that are unobservable in historic and contemporary field sampling efforts. The NLA represents the current best-practice in large scale field monitoring across the U.S.; however, we show that lake clarity nationally has distinct temporal patterns that are not fully captured with the 5-year return period of the NLA

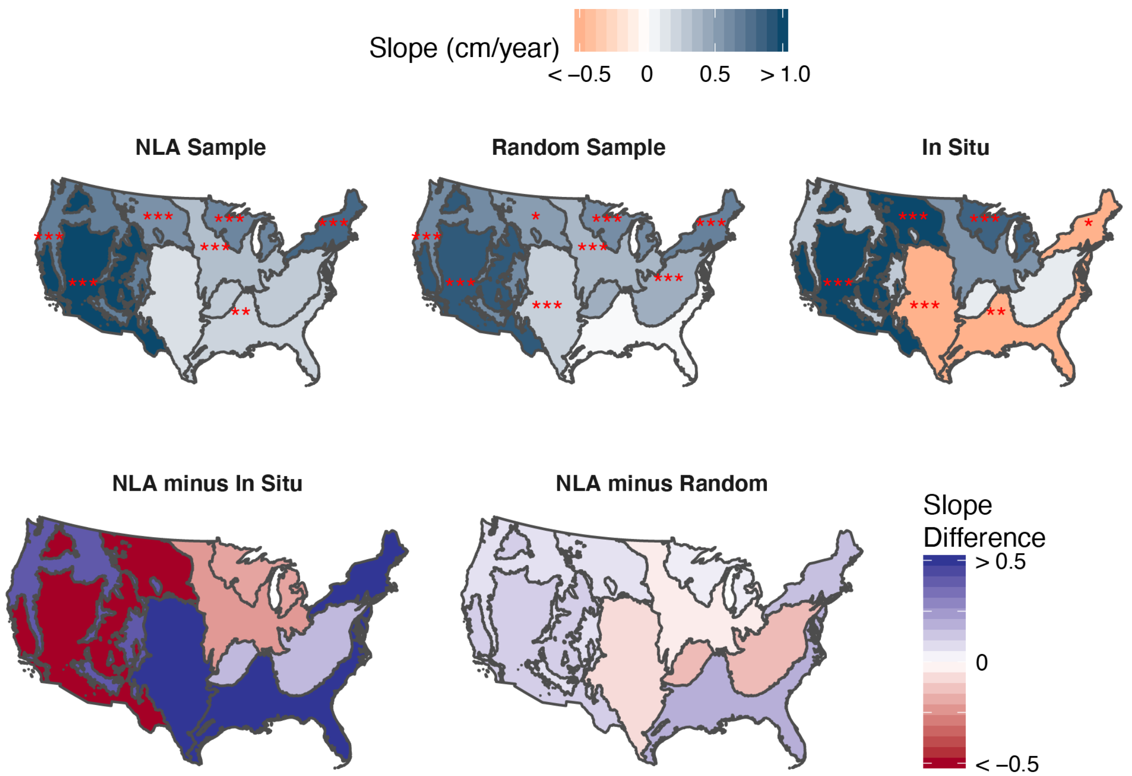

Figure 4. Differences in observed ecoregion trends when conducting the analysis with all the in situ samples from the WQP/LAGOS-NE and the modelling results from the NLA lake sample and a large random sample. Asterisks indicate significance levels of trends determined by Thiel-Sen slopes at 90% (*), 95% (**), and 99% (***) confidence levels.

field sampling efforts. High correlations between trends observed with different lake samples, high correlations in time series among regions, and periods of uniform change at the national scale all point to the influence of one or more drivers of lake water clarity operating at a national scale or larger. We examined relationships between observed water clarity patterns and potential forcing variables (temperature, precipitation, sulfate deposition, and the Pacific Decadal Oscillation, Figure S10) and found that the regional impacts of these correlations varied, likely due to complex, cross-scale interactions that lead to variable regional influences as different drivers interact with each other (3,26,39). However, while more difficult to quantify, the period analyzed here begins directly after a round of sweeping environmental legislation in the 1970s and 1980s. These major national level policies include the Clean Water Act (CWA 1972; amended 1977 and 1987), the National Environmental Policy Act (NEPA 1969), the Clean Air Act (CAA 1963, amended 1965, 1966, 1967, 1969, 1970, 1977, 1990), the Safe Water Drinking Act (SWDA 1974, amended 1986,1996), and the Endangered Species Act (ESA 1973), all of which targeted freshwater resources and habitat to varying extents.

Our results are consistent with recent studies showing regional (46,47) and national (41,42) improvements to U.S. streams and rivers (41,42,46,47) and lakes (42) directly attributable to the CWA. Specifically, they show declining nutrient concentrations in urban areas caused by reductions in point source pollution and improved stormwater management emphasized by the CWA. Although agricultural streams have not undergone significant changes in nutrient loads, they have shown declines in suspended sediments, consistent with improved sediment management practices (41). These recorded improvements in streams and rivers provide a mechanism for increasing lake water clarity, as changes in fluvial systems often equate to changes in sediment and nutrient inputs to lakes (48). This argument assumes that the observed improvements in clarity can be attributed to declining suspended sediment and nutrient concentrations rather than the other contributor to water clarity – 'colored' dissolved organic matter (cDOM) because where cDOM patterns exist in lakes, they are predominantly positive (49) and therefore not contributing to increases in clarity.

Evaluating long-term nutrient dynamics is more challenging because of limitations in data availability over the period of study at the national scale. An analysis of the 17-state region represented by the LAGOS database revealed that total nitrogen decreased while total phosphorus concentrations have neither decreased nor increased in the vast majority of lakes sampled during summer months between 1990 and 2013 (50). While this nutrient decrease alone potentially contributed to increased lake clarity in nitrogen-limited waterbodies, the study lacks lake water quality data that corresponds to the period of greatest change observed in streams, which was steepest from 1982-1992 within urban areas (41). The diminishing improvements in stream water quality after this period are likely because investment in municipal and industrial water pollution control efforts began to gradually taper off in the mid-1990s (51). Even allowing for a delay in water quality response to phosphorus reductions (43), these funding patterns are consistent with the greatest gains in water clarity occurring over the first two decades of the CWA within lakes in densely settled areas and smaller waterbodies that tend to be more responsive to management activities because of their shorter average water residence times. Our results support this conclusion, with smaller lakes showing over three times the median increase in clarity than larger lakes ($p = 4.7e^{-8}$), with lakes in catchments with higher population density showing over four times the median increase in clarity than lakes in low population density catchments ($p = 2.2e^{-16}$) (Figure 3), and a slowdown of clarity improvements after 2000 due to diminishing returns of reduced point source pollution. This slowdown was likely exacerbated due to difficulties reducing nonpoint sources of pollution, particularly in some regions of the country where changes in the precipitation regime are exacerbating nutrient loading to surface waters (52).

Comparison of observed trends across the NLA sample of lakes, a large random sample, and historical field records provides both empirical support for the representativeness of the NLA and evidence for the shortcomings of relying solely on potentially biased historical field samples for systematic monitoring of freshwater resources. Examining trends at the lake and regional level highlights the potential for an unrepresentative sample of lakes to inaccurately depict system-wide patterns. Specifically, when we restrict analysis to larger waterbodies, we find only nominal change in U.S. lake clarity, but the more inclusive analysis presented here suggests that overall lake water clarity within the United States has increased over the past 35 years. While this is the first study of trends in lake water clarity at a national scale, it extends regional studies throughout the northeast that have found water quality in lakes is either largely stable or improving (50,53–55), as well as work in China and Sweden indicating that national management policies are decreasing eutrophication rates (4,56,57). While more work is required to understand the multiscale drivers of water clarity, the results presented here bring us closer to realizing research goals dating back more than 20 years emphasizing that representative sampling is required for effective monitoring of freshwater resources (6,7).

References:

1. Filazzola A, Mahdiyan O, Shuvo A, Ewins C, Moslenko L, Sadid T, et al. A database of chlorophyll and water chemistry in freshwater lakes. Sci Data. 2020 Sep 22;7(1):310.

2. Soranno PA, Bacon LC, Beauchene M, Bednar KE, Bissell EG, Boudreau CK, et al. LAGOS-NE: A multi-scaled geospatial and temporal database of lake ecological context and water quality for thousands of U.S. lakes. GigaScience. 2017;(October 2017):1–22.

3. Read EK, Carr L, De Cicco L, Dugan HA, Hanson PC, Hart JA, et al. Water quality data for national-scale aquatic research: The Water Quality Portal. Water Resour Res. 2017 Feb;53(2):1735–1745.

4. Fölster J, Johnson RK, Futter MN, Wilander A. The Swedish monitoring of surface waters: 50 years of adaptive monitoring. AMBIO. 2014 Dec;43(S1):3–18.

5. Stanley EH, Collins SM, Lottig NR, Oliver SK, Webster KE, Cheruvelil KS, et al. Biases in lake water quality sampling and implications for macroscale research. Limnol Oceanogr. 2019;64(4):1572–85.

6. Peterson SA, Urquhart NS, Welch EB. Sample representativeness: A must for reliable regional lake condition estimates. Environ Sci Technol. 1999;33(10):1559–1565.

7. Paulsen SG, Hughes RM, Larsen DP. Critical elements in describing and understanding our nation's aquatic resources. J Am Water Resour Assoc. 1998;34(5):995–1005.

8. Pollard AI, Hampton SE, Leech DM. The promise and potential of continental-scale limnology using the U.S. Environmental Protection Agency's National Lakes Assessment. Limnol Oceanogr Bull. 2018;27(2):36–41.

9. Hughes RM, Peck DV. Acquiring data for large aquatic resource surveys: the art of compromise among science, logistics, and reality. J North Am Benthol Soc. 2008;27(4):837–859.

10. Topp SN, Pavelsky TM, Jensen D, Simard M, Ross MRV. Research trends in the use of remote sensing for inland water quality science: moving towards multidisciplinary applications. Water. 2020 Jan;12(1):169.

11. Ho JC, Michalak AM, Pahlevan N. Widespread global increase in intense lake phytoplankton blooms since the 1980s. Nature. 2019;574(7780):667–670.

12. Olmanson LG, Bauer ME, Brezonik PL. A 20-year Landsat water clarity census of Minnesota's 10,000 lakes. Remote Sens Environ. 2008;112(11):4086–4097.

13. Peck DV, Olsen AR, Weber MH, Paulsen SG, Peterson C, Holdsworth SM. Survey design and extent estimates for the National Lakes Assessment. Freshw Sci. 2013 Oct;32(4):1231–45.

14. McKay L, Bondelid T, Dewald T, Johnston J, Moore R, Rea A. NHDPlus Version 2: User Guide. US EPA; 2019.

15. Ross MRV, Topp SN, Appling AP, Yang X, Kuhn C, Butman D, et al. AquaSat: A data set to enable remote sensing of water quality for inland waters. Water Resour Res. 2019;55(11):10012–25.

16. Griffin CG, McClelland JW, Frey KE, Fiske G, Holmes RM. Quantifying CDOM and DOC in major Arctic rivers during ice-free conditions using Landsat TM and ETM+ data. Remote Sens Environ. 2018 May 1;209:395–409.

17. Kuhn C, de Matos Valerio A, Ward N, Loken L, Sawakuchi HO, Kampel M, et al. Performance of Landsat-8 and Sentinel-2 surface reflectance products for river remote sensing retrievals of chlorophyll-a and turbidity. Remote Sens Environ. 2019 Apr;224:104–18.

18. Olmanson LG, Page BP, Finlay JC, Brezonik PL, Bauer ME, Griffin CG, et al. Regional measurements and spatial/temporal analysis of CDOM in 10,000+ optically variable Minnesota lakes using Landsat 8 imagery. Sci Total Environ. 2020 Jul 1;724:138141.

19. Hill RA, Weber MH, Debbout RM, Leibowitz SG, Olsen AR. The Lake-Catchment (LakeCat) Dataset: characterizing landscape features for lake basins within the conterminous USA. Freshw Sci. 2018;37(March):208–21.

20. Jones JW. Improved automated detection of subpixel-scale inundation—revised dynamic surface water extent (DSWE) partial surface water tests. Remote Sens. 2019 Jan;11(4):374.

21. Zhu Z, Wang S, Woodcock CE. Improvement and expansion of the Fmask algorithm: Cloud, cloud shadow, and snow detection for Landsats 4-7, 8, and Sentinel 2 images. Remote Sens Environ. 2015;159:269–277.

22. Gorelick N, Hancher M, Dixon M, Ilyushchenko S, Thau D, Moore R. Google Earth Engine: Planetary-scale geospatial analysis for everyone. Remote Sens Environ. 2017;

23. Gardner JR, Yang X, Topp SN, Ross MRV, Altenau EH, Pavelsky TM. The Color of Rivers. Geophys Res Lett. 2020;e2020GL088946.

24. Randles CA, da Silva AM, Buchard V, Colarco PR, Darmenov A, Govindaraju R, et al. The MERRA-2 aerosol reanalysis, 1980 onward. Part I: System description and data assimilation evaluation. J Clim. 2017 Apr 12;30(17):6823–50.

25. Wang S, Li J, Shen Q, Zhang B, Zhang F, Lu Z. MODIS-Based radiometric color extraction and classification of inland water with the forel-ule scale: A case study of lake Taihu. IEEE J Sel Top Appl Earth Obs Remote Sens. 2015;8(2):907–918.

26. Rose KC, Greb SR, Diebel M, Turner MG. Annual precipitation regulates spatial and temporal drivers of lake water clarity: Ecol Appl. 2017;27(2):632–643.

27. Lottig NR, Tan PN, Tylerwagner T, Cheruveli KS, Soranno PA, Stanley EH, et al. Macroscale patterns of synchrony identify complex relationships among spatial and temporal ecosystem drivers. Ecosphere. 2017;8(12).

28. Li M, Ma L, Blaschke T, Cheng L, Tiede D. A systematic comparison of different object-based classification techniques using high spatial resolution imagery in agricultural environments. Int J Appl Earth Obs Geoinformation. 2016;49:87–98.

29. Georganos S, Grippa T, Vanhuysse S, Lennert M, Shimoni M, Wolff E. Very high resolution object-based land use-land cover urban classification using extreme gradient boosting. IEEE Geosci Remote Sens Lett. 2018 Apr;15(4):607–611.

30. Just A, De Carli M, Shtein A, Dorman M, Lyapustin A, Kloog I. Correcting measurement error in satellite aerosol optical depth with machine learning for modeling PM2.5 in the Northeastern USA. Remote Sens. 2018;10(5):803.

31. Fan J, Wang X, Wu L, Zhou H, Zhang F, Yu X, et al. Comparison of Support Vector Machine and Extreme Gradient Boosting for predicting daily global solar radiation using temperature and precipitation in humid subtropical climates: A case study in China. Energy Convers Manag. 2018;164(January):102–111.

32. Meyer H, Reudenbach C, Hengl T, Katurji M, Nauss T. Improving performance of spatio-temporal machine learning models using forward feature selection and target-oriented validation. Environ Model Softw. 2018;101:1–9.

33. Meyer H, Reudenbach C, Wöllauer S, Nauss T. Importance of spatial predictor variable selection in machine learning applications – Moving from data reproduction to spatial prediction. 2019; Available from: http://arxiv.org/abs/1908.07805

34. Apley DW, Zhu J. Visualizing the effects of predictor variables in black box supervised learning models. J R Stat Soc Ser B. 2020;82(4):1059–86.

35. Sen PK. Estimates of the regression coefficient based on Kendall's Tau. J Am Stat Assoc. 1968 Dec;63(324):1379–89.

36. Kendall MG. Rank correlation methods. Oxford, England: Griffin; 1948. (Rank correlation methods).

37. Ren J, Zheng Z, Li Y, Lv G, Wang Q, Lyu H, et al. Remote observation of water clarity patterns in Three Gorges Reservoir and Dongting Lake of China and their probable linkage to the Three Gorges Dam based on Landsat 8 imagery. Sci Total Environ. 2018;625:1554–1566.

38. Page BP, Olmanson LG, Mishra DR. A harmonized image processing workflow using Sentinel-2/MSI and Landsat-8/OLI for mapping water clarity in optically variable lake systems. Remote Sens Environ. 2019 Sep;231:111284.

39. Soranno PA, Cheruvelil KS, Bissell EG, Bremigan MT, Downing JA, Fergus CE, et al. Cross-scale interactions: Quantifying multi-scaled cause-effect relationships in macrosystems. Front Ecol Environ. 2014;12(1):65–73.

40. O'Neil JM, Davis TW, Burford MA, Gobler CJ. The rise of harmful cyanobacteria blooms: The potential roles of eutrophication and climate change. Harmful Algae. 2012 Feb 1;14:313–34.

41. Stets EG, Sprague LA, Oelsner GP, Johnson HM, Murphy JC, Ryberg K, et al. Landscape drivers of dynamic change in water quality of U.S. rivers. Environ Sci Technol. 2020 Mar 27;54:4336–43.

42. Keiser DA, Shapiro JS. Consequences of the Clean Water Act and the demand for water quality. Q J Econ. 2019 Feb 1;134(1):349–96.

43. Jeppesen E, Søndergaard M, Jensen JP, Havens KE, Anneville O, Carvalho L, et al. Lake responses to reduced nutrient loading - An analysis of contemporary long-term data from 35 case studies. Freshw Biol. 2005;50(10):1747–1771.

44. Schindler DW. Recent advances in the understanding and management of eutrophication. Limnol Oceanogr. 2010;51(1part2):356–363.

45. Downing JA, Prairie YT, Cole JJ, Duarte CM, Tranvik LJ, Striegl RG, et al. The global abundance and size distribution of lakes, ponds, and impoundments. Limnol Oceanogr. 2006;51(5):2388–2397.

46. Wong WH, Dudula JJ, Beaudoin T, Groff K, Kimball W, Swigor J. Declining ambient water phosphorus concentrations in Massachusetts' rivers from 1999 to 2013: Environmental protection works. Water Res. 2018 Aug;139:108–17.

47. Ator SW, García AM, Schwarz GE, Blomquist JD, Sekellick AJ. Toward explaining nitrogen and phosphorus trends in Chesapeake Bay tributaries, 1992–2012. JAWRA J Am Water Resour Assoc. 2019;55(5):1149–68.

48. Fraterrigo JM, Downing JA. The influence of land use on lake nutrients varies with watershed transport capacity. Ecosystems. 2008 Nov 1;11(7):1021–34.

49. Monteith DT, Stoddard JL, Evans CD, de Wit HA, Forsius M, Høgåsen T, et al. Dissolved organic carbon trends resulting from changes in atmospheric deposition chemistry. Nature. 2007 Nov;450(7169):537–40.

50. Oliver SK, Collins SM, Soranno PA, Wagner T, Stanley EH, Jones JR, et al. Unexpected stasis in a changing world: Lake nutrient and chlorophyll trends since 1990. Glob Change Biol. 2017;23(12):5455–5467.

51. Keiser DA, Kling CL, Shapiro JS. The low but uncertain measured benefits of US water quality policy. Proc Natl Acad Sci. 2019 Mar 19;116(12):5262–9.

52. Ballard TC, Sinha E, Michalak AM. Long-term changes in precipitation and temperature have already impacted nitrogen loading. Environ Sci Technol. 2019 May 7;53(9):5080–90.

53. Binding CE, Greenberg TA, Watson SB, Rastin S, Gould J. Long term water clarity changes in North America's Great Lakes from multi-sensor satellite observations. Limnol Oceanogr. 2015 Nov;60(6):1976–1995.

54. Peckham SD, Lillesand TM. Detection of spatial and temporal trends in Wisconsin lake water clarity using landsat-derived estimates of secchi depth. Lake Reserv Manag. 2006;22(4):331–341.

55. Canfield DE, Bachmann RW, Stephens DB, Hoyer MV, Bacon L, Williams S, et al. Monitoring by citizen scientists demonstrates water clarity of Maine (USA) lakes is stable, not declining, due to cultural eutrophication. Inland Waters. 2016;6(1):11–27.

56. Wang S, Li J, Zhang B, Lee Z, Spyrakos E, Feng L, et al. Changes of water clarity in large lakes and reservoirs across China observed from long-term MODIS. Remote Sens Environ. 2020 Sep 15;247:111949.

57. Ma T, Zhao N, Ni Y, Yi J, Wilson JP, He L, et al. China's improving inland surface water quality since 2003. Sci Adv. 2020 Jan 1;6(1):eaau3798.

Acknowledgments: We would like to thank the reviewers that contributed feedback to this manuscript.

Funding: Funding for this work came from NASA NESSF Grant 80NSSC18K1398. The contributions from EHS were supported by the National Science Foundation grant EF-1685534.

Author contributions: SNT conducted modelling, data analysis, and manuscript preparation. SNT, TMP, MRVR, and XY contributed to study design. EHS and CGG contributed limnology and remote sensing expertise respectively. All authors contributed significant manuscript feedback and edits.

Competing interests: The authors declare no conflicts of interest in regards to this manuscript.

Data availability:. The DSWE variant of AquaSat used in this analysis can be found on figshare (doi: 10.6084/m9.figshare.12227273). Additional data used for this paper come from LAGOS-NE (doi:10.6073/pasta/0c23a789232ab4f92107e26f70a7d8ef), LakeCAT (ftp://newftp.epa.gov/EPADataCommons/ORD/NHDPlusLandscapeAttributes/LakeCat/FinalTables/), NHDPlusV2 (https://www.epa.gov/waterdata/nhdplus-national-data), and the Water Quality Portal (https://www.waterqualitydata.us/portal/).

Code availability: All code for the analysis can be found at https://github.com/SimonTopp/USLakeClarityTrendr.

Supplemental Material for

Multi-Decadal Improvement in U.S. Lake Water Clarity

Simon N. Topp*[1], Tamlin M. Pavelsky[1], Emily H. Stanley[2], Xiao Yang[1], Claire G. Griffin[3], Matthew R.V. Ross[4].

[1] Department of Geological Sciences, University of North Carolina at Chapel Hill

[2] Center for Limnology, University of Wisconsin-Madison

[3] Department of Environmental Sciences, University of Virginia

[4] Department of Ecosystem Science and Sustainability, Colorado State University

*Correspondence to: sntopp@live.unc.edu

This PDF file includes:

Figures S1-S10

Table S1

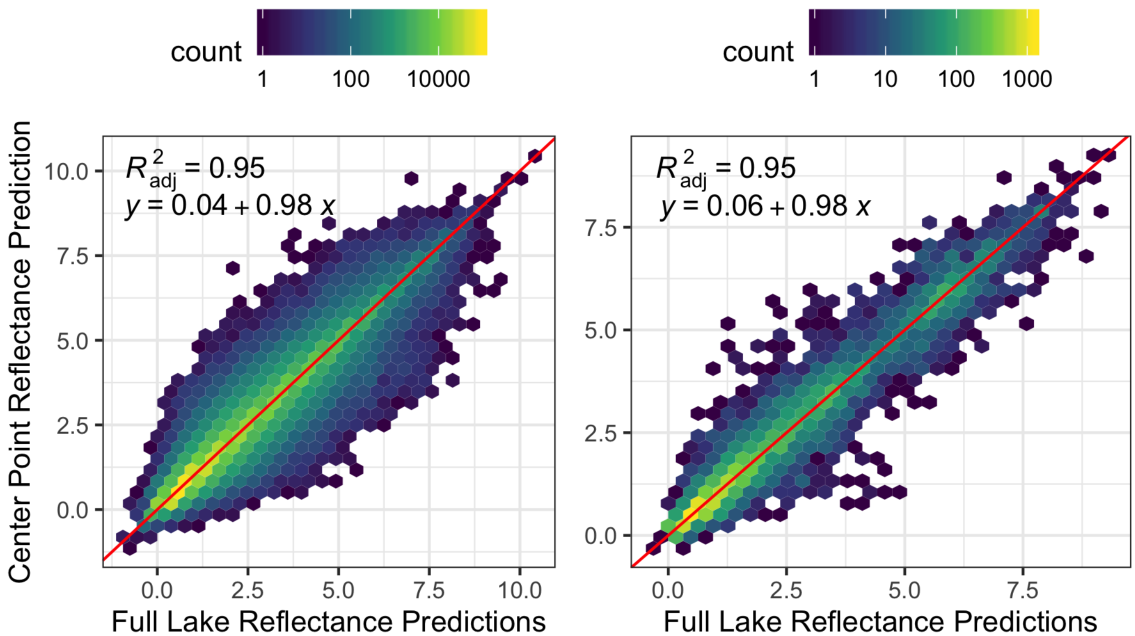

Figure S1. Comparison of predictions using median reflectance values from a buffered lake center point and median reflectance values from the entire lake polygon for (left) the full NLA 2012 sample of lakes and (right) NLA lakes over 10 km^2 where there is the highest potential difference for variation between center point and full lake reflectance values. Red line indicates 1:1 while the color indicates the density of points for a given location.

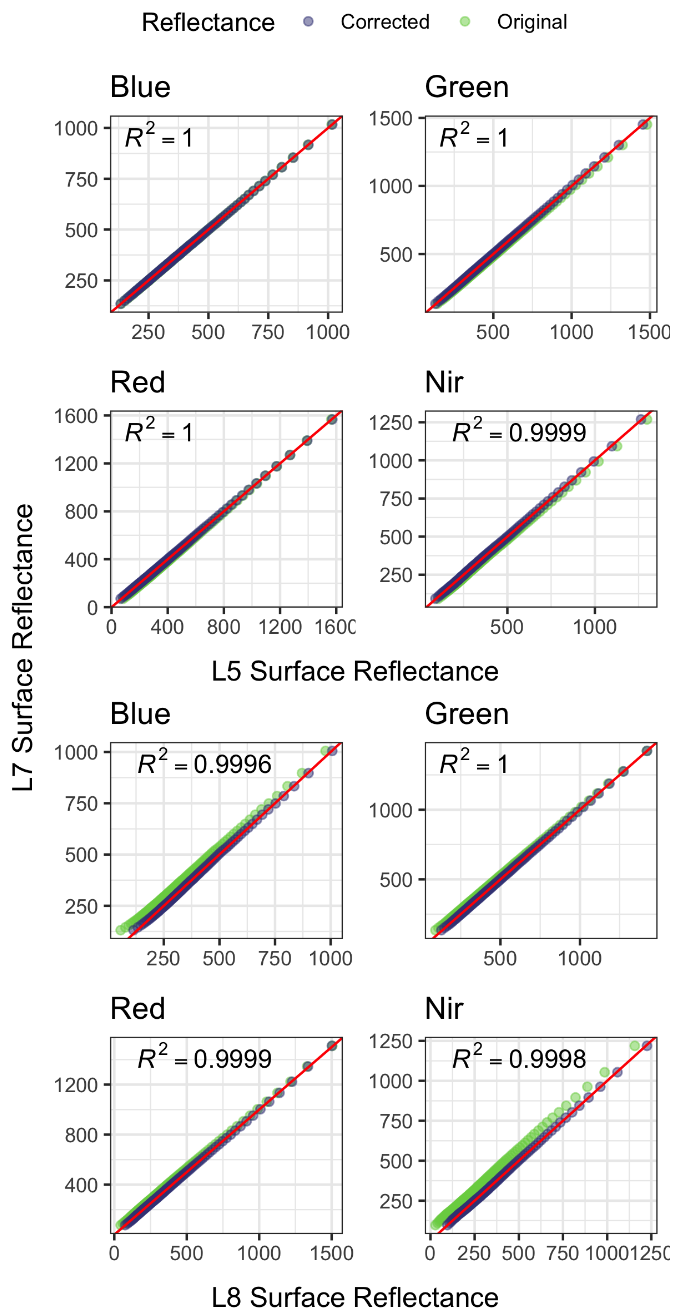

Figure S2. Results of sensor corrections for Landsat 5 and Landsat 8 to Landsat 7 values. Reflectance values from the 1st-99th percentile were taken from the distributions of values during coincident flight years over the entirety of the NLA dataset (n = 1,029 lakes) and corrected to Landsat 7 values through second order polynomial regression. Red lines are 1:1 lines and R^2 values are for corrected reflectance and Landsat 7 reflectance.

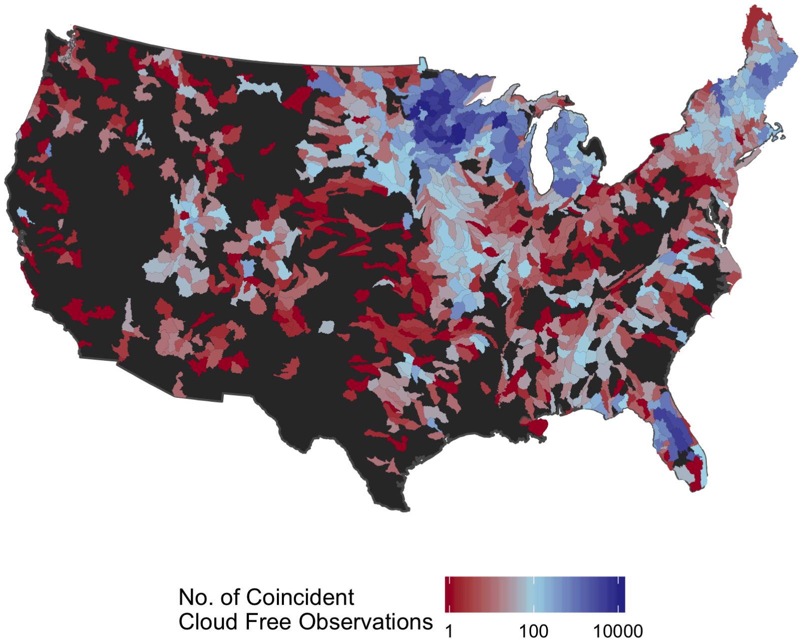

Figure S3. Distribution of coincident satellite and field observations used for model training and validation aggregated by HUC 8 watershed. Distributions largely follow the geographical concentration of lakes.

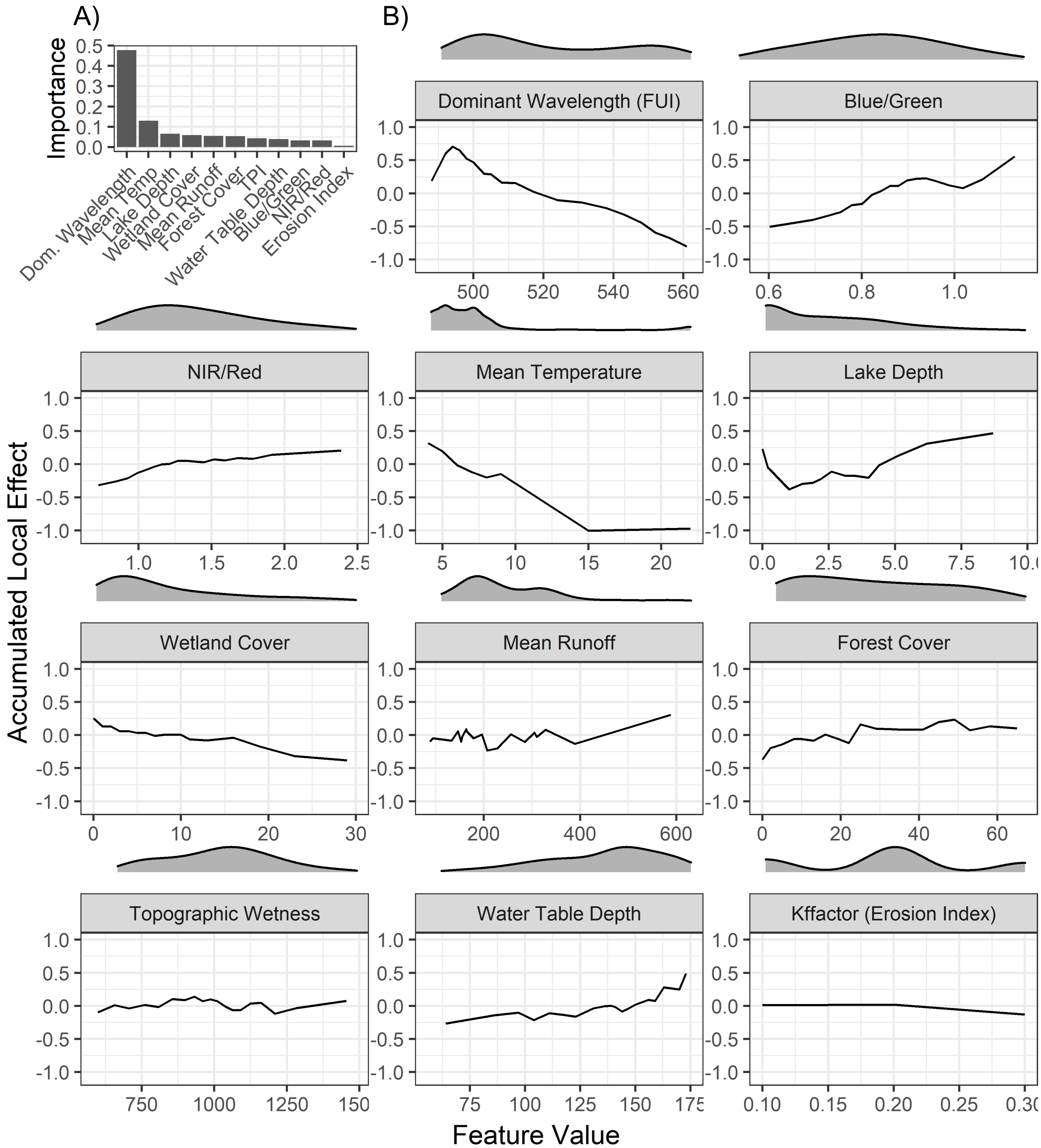

Figure S4. A) Feature importance as measured by model gain for all the model inputs. B) Accumulated local effects (ALE) for each feature. ALE values show the average impact to model predictions as you move along localized window of feature values. Density distribution plots above the ALE plots show the distribution of each feature (5^{th}-95^{th} percentile) within the training set.

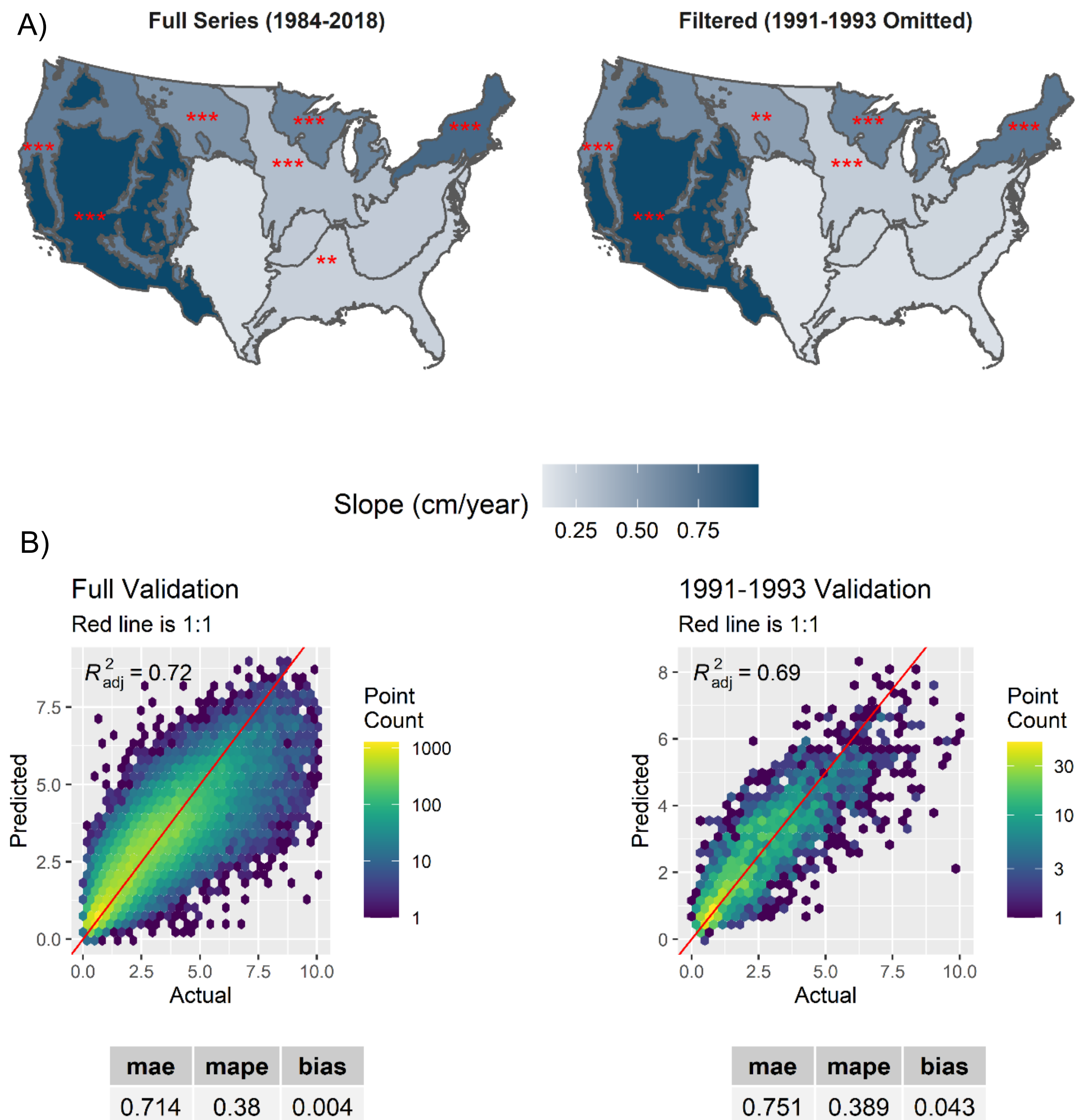

Figure S5. A) Comparison of estimated Sen Slopes for the 2012 NLA sample of lakes for the full timeseries and omitting years with high atmospheric optical depth due to the Mt. Pinatubo eruption. Trends for all regions remain positive within the filtered timeseries and only one region, the Coastal Plains, is no longer statistically significant at a 95% confidence interval. B) Hold-out validation metrics for the full timeseries compared to 1991-1993. Bias is ~4 cm higher in 1991-1993, indicating that if anything clarity is slightly underpredicted for the years in question compared to the full time period.

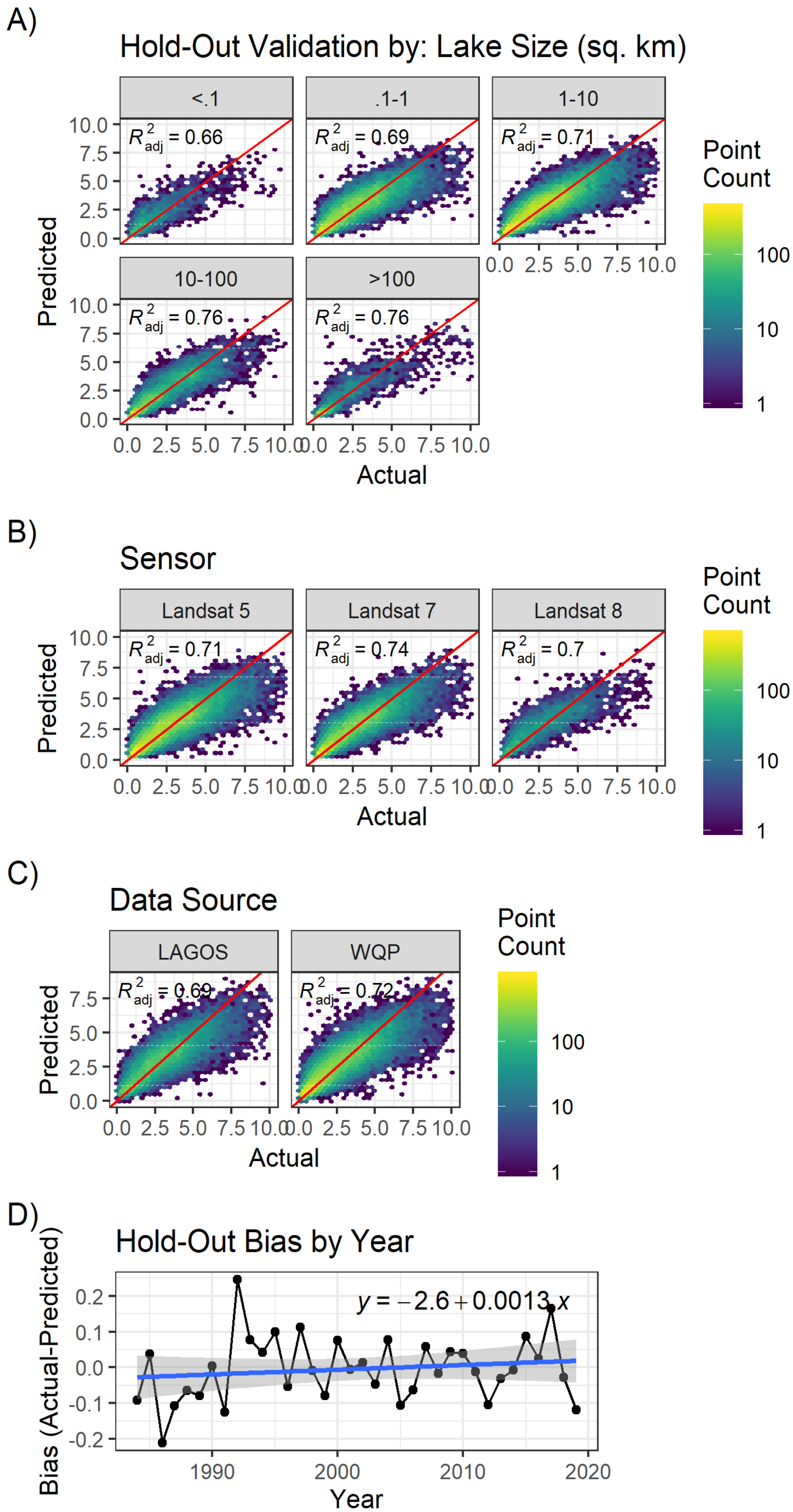

Figure S6. Breakdown of model validation by (A) lake size, (B) sensor, (C) data source, and (D) time. Red lines represent 1:1 lines.

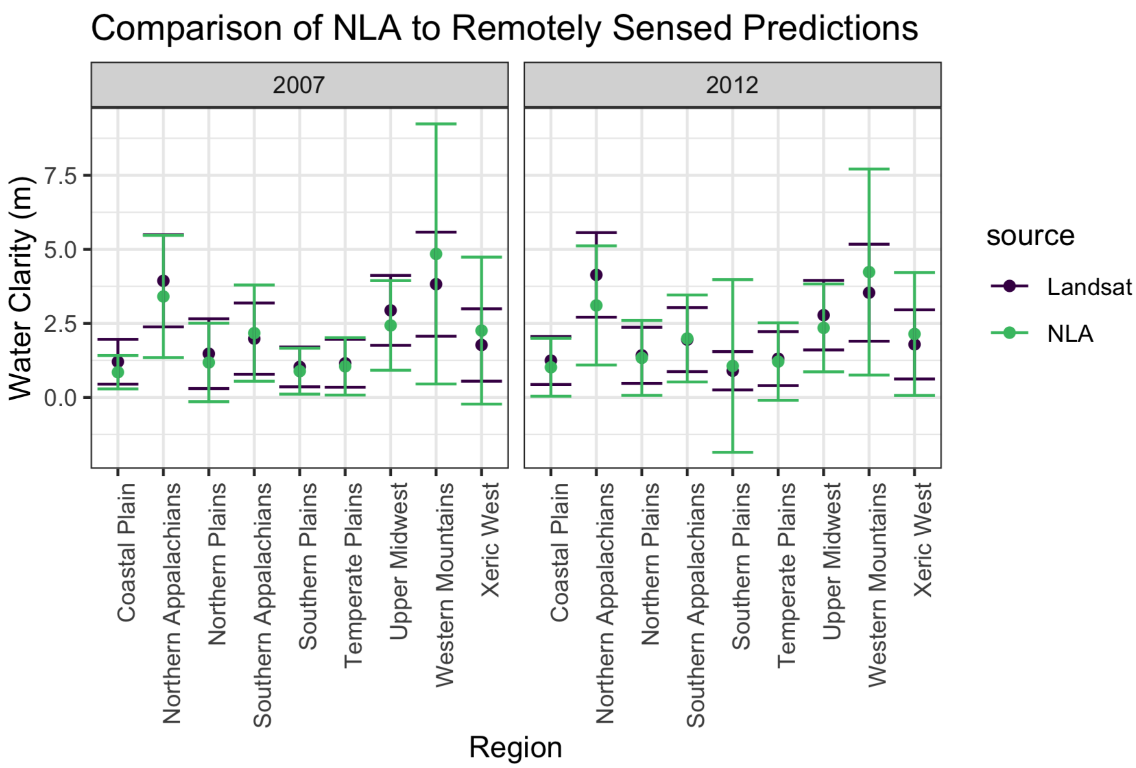

Figure S7. Comparison of predicted regional summer water clarity values with field measurements from the 2007 NLA (left) and 2012 NLA (right). Points represent regional means and error bars represent one standard deviation.

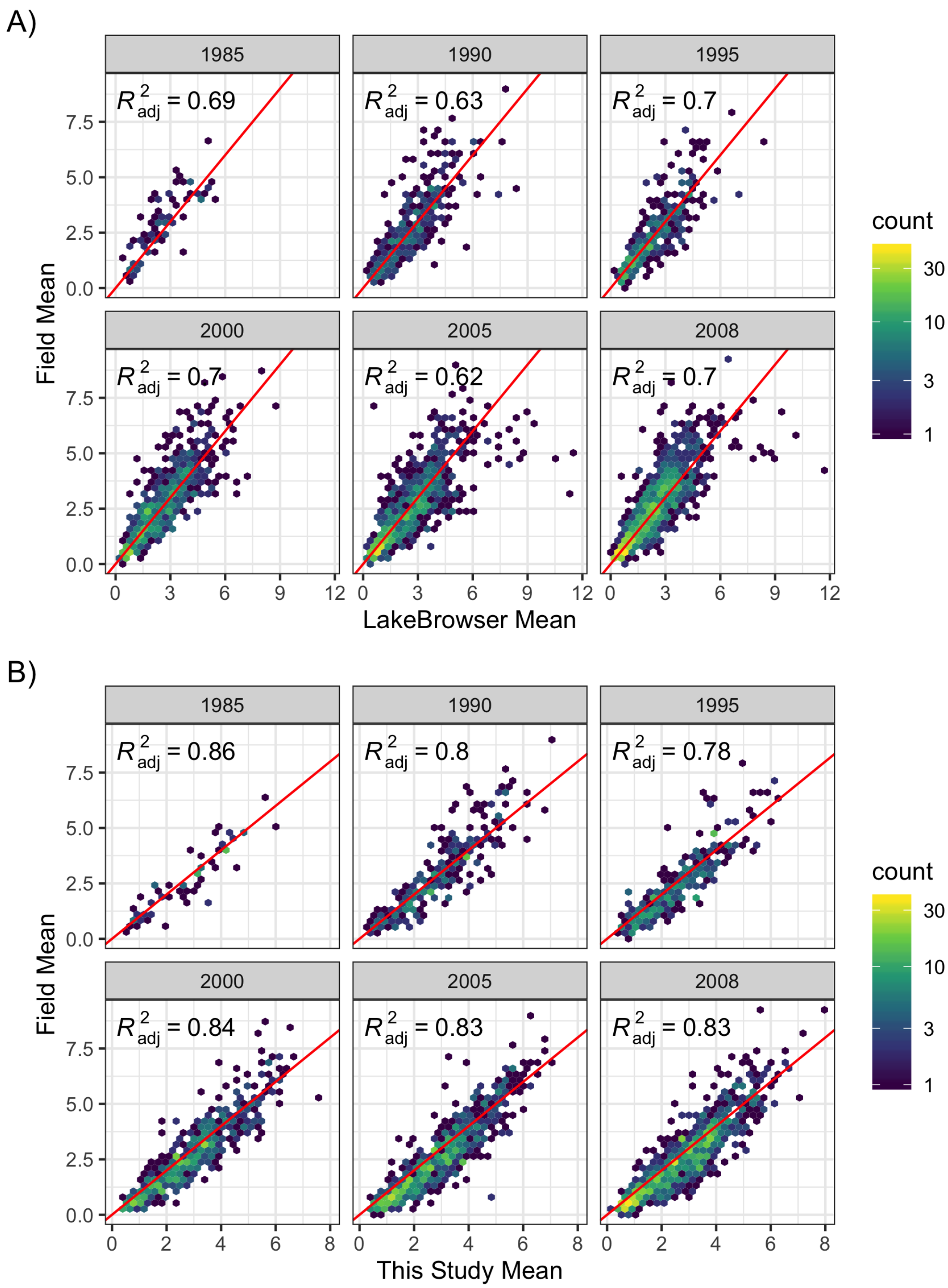

Figure S8. Comparison of predicted mean annual clarity for individual lakes from (A) LakeBrowser and (B) this study for those lakes/years with field data from the Water Quality Portal or LAGOS-NE. Predictions from LakeBrowser are those available from their data portal and represent the mean clarity estimate from 1-2 Landsat scenes per year. This study's predictions were derived by filtering cloud free Landsat scenes for each year down to only those months considered by LakeBrowser; however, since specific source scene data is unavailable from LakeBrowser, our summer estimates are the mean of all available scenes in the coincident time period (generally 2-4 scenes per lake per year), and therefore do not exactly match those from LakeBrowser.

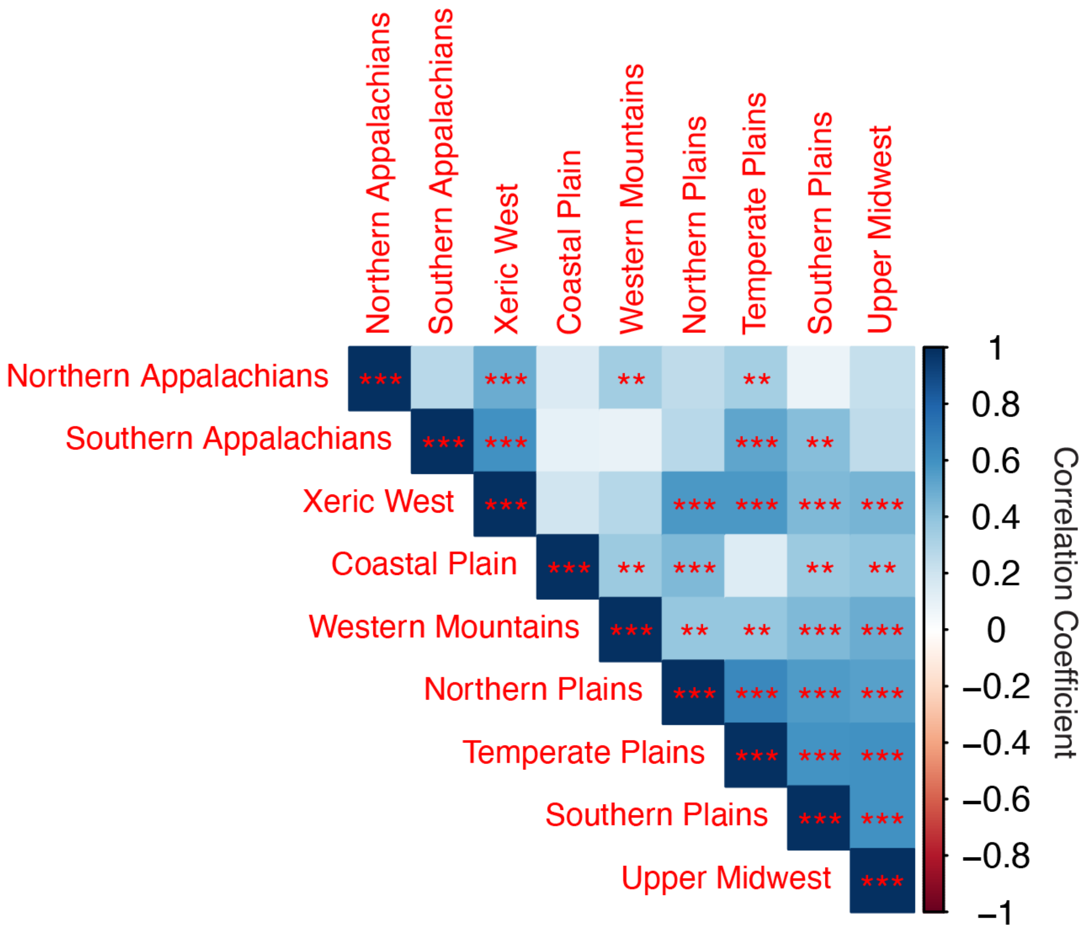

Figure S9. Pearson's correlation matrix for time series between regions using the NLA sample of lakes. One, two, and three asterisks represent significance at the 90th, 95th, and 99th percent confidence intervals respectively

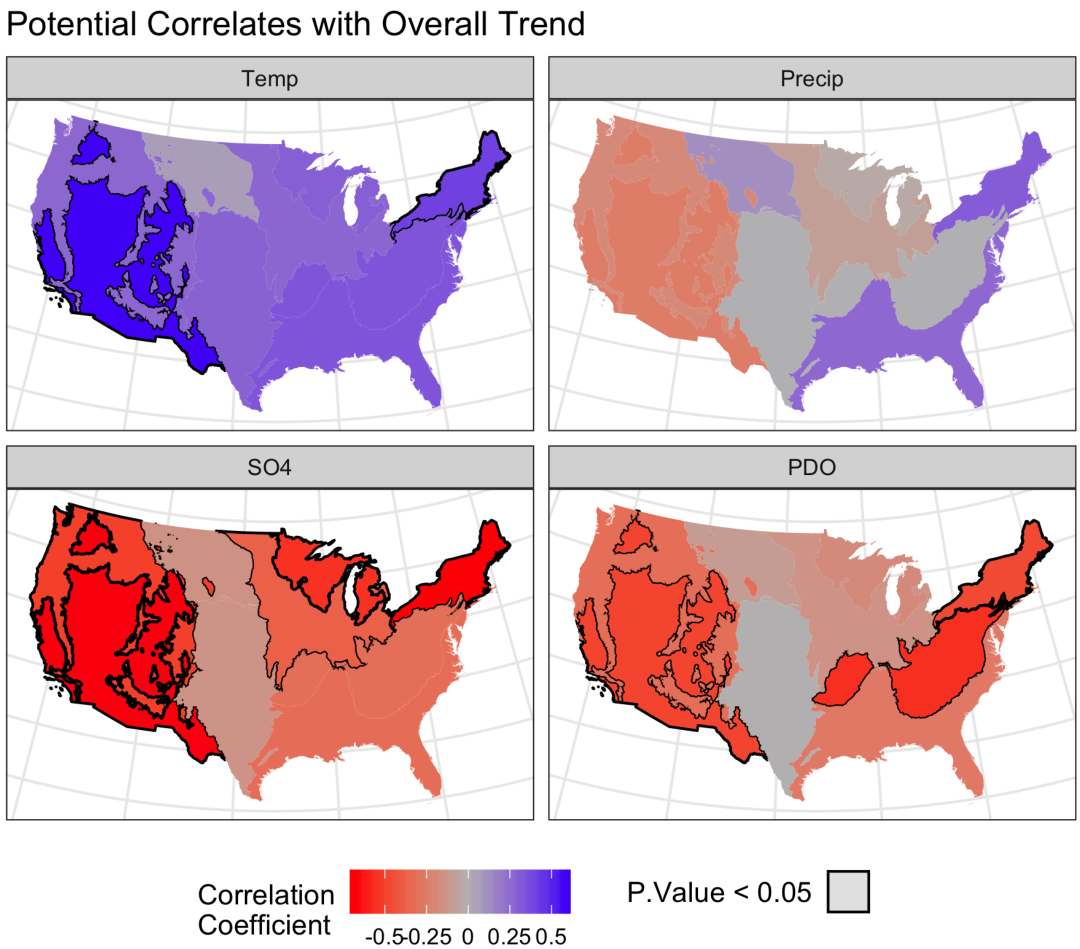

Figure S10. Ecoregion scale correlations. Clockwise from the top left: Ecoregion mean annual summer temperature from PRISM, Ecoregion mean annual summer precipitation from PRISM, Pacific Decadal Oscillation, and mean regional SO4 deposition from the National Atmospheric Deposition Program.

Variable	Description
Lake Area	Lake area from NHD v2 (sq. km)
Lake Depth	**Mean lake depth from NHD v2 (m)**
NIR/Red	**Band Ratio**
Blue/Green	**Band Ratio**
Forel-Ule Index	**Dominant Color Wavelength as defined by Wang et al. (2015)**
Network Status	Binary on/off network status for lake based on NHD flowlines
Percent Carbonate	Percent of catchment area classified as lithology type: carbonate residual material
Mean Precipitation	PRISM climate data - 30-year normal mean precipitation (mm): Annual period: 1981-2010 within the catchment
Mean Temperature	**PRISM climate data - 30-year normal mean temperature (C°): Annual period: 1981-2010 within the catchment**
Runoff	**Mean runoff (mm) within catchment**
Percent Clay	Mean % clay content of soils (STATSGO) within catchment
Percent Sand	Mean % sand content of soils (STATSGO) within catchment
Percent Organic Matter	Mean organic matter content (% by weight) of soils (STATSGO) within catchment
Soil Permeability	Mean permeability (cm/hour) of soils (STATSGO) within catchment
Bedrock Depth	Mean depth (cm) to bedrock of soils (STATSGO) within catchment
Water Table Depth	**Mean seasonal water table depth (cm) of soils (STATSGO) within catchment**
Base Flow Index	Base flow is the component of streamflow that can be attributed to ground-water discharge into streams. The BFI is the ratio of base flow to total flow, expressed as a percentage, within catchment
Elevation	Mean catchment elevation (m)
Atmospheric Optical Depth	Atmospheric Optical Depth over observation pulled from MERRA 2 reanalysis data
Kffactor	**Mean of STATSGO Kffactor raster within catchment. The Universal Soil Loss Equation (USLE) and represents a relative index of susceptibility of bare, cultivated soil to particle detachment and transport by rainfall**
Catchement Area	Area of local catchment (square km)
Percent Agriculture	% of catchment area classified as ag land cover (NLCD 2006 classes 81-82) occurring on slopes > 10%
NPDE Density	Density of permitted NPDES (National Pollutant Discharge Elimination System) sites within catchment (sites/square km)
Hydraulic Conductivity	Mean lithological hydraulic conductivity (micrometers per second) content in surface or near surface geology within catchment
Percent Impervious Surface	Mean imperviousness of anthropogenic surfaces within catchment (NLCD 2006)
Percent Urban	Percent of catchment classified as either medium or high density urban (NLCD 2006)
Percent Forest	**Percent of catchment classified as either deciduous, coniferous, or mixed forest (NLCD 2006)**
Percent Crop	Percent of catchment area classified as crop land use (NLCD 2006 class 82)
Percent Wetland	**Percent of catchment classified as woody or herbaceous wetland landcover (NLCD 2006)**
Topographic Wetness Index	**Mean Composite Topographic Index (CTI)[Wetness Index] within catchment**

Table S1.

Variables included in modelling pipeline. Variables included in the final model after FFS with LLLTO-CV procedure are indicated in bold.